CHAPTER III

Synthesis of Carbohydrate–conjugate Heterobimetallic Cu^{II}-Sn^{IV}_2 and Zn^{II}-Sn^{IV}_2 Complexes; Their Interactions with CT DNA and Nucleotides; DNA cleavage, *in-vitro* Cytotoxicity.

Synthesis

Synthesis of the tet(GLcN)$_2$

The ligand was prepared by adopting the procedure reported earlier with slight modification [211,212]. A methanolic solution (20 mL) containing 1,8-diamino-3,6-diazaoctane (0.149 mL, 1mmol) and D-glucosamine (0.430 g, 2.0 mmol) were refluxed at 80 °C for 1.5 h. The mixture turned pale yellow transparent solution. The completion of the reaction was monitored with the help of TLC. The product was obtained as a pale yellow liquid.

^{1}H NMR (400MHz, D_2O, δ): 5.20 (NH_2 GlcN, 4H); 3.87 - 2.78 (OH,CH_2,CH, NH, of GLcN-tet, 36H). ^{13}C NMR (100 MHz, D_2O, δ): 74.43, 74.33, 73.40, 71.38, 71.31, 71.03, 70.11, 62.40, 62.36, 53.37, 51.36, 49.86 (12 C, GlcN); 49.68, 49.61, 49.08, 49.01, 48.93, 45.59 (6 C, amine). ESI-MS:(m/z, H_2O): 472 $[C_{18}H_{40}N_6O_8 + 3H]^+$.

Synthesis of tet(GLcN)$_2$Ni(Im)$_2$Sn$_2$

To the methanolic solution of the ligand (0.469 g, 1mmol), bis(imidazole)nickel(II) chloride (0.265 g, 1 mmol) was added [213]. The resulting blue colored solution was stirred for 2 h. To the above reaction mixture, $SnCl_4.5H_2O$ (0.704 g, 2 mmol) dissolved in MeOH was added and stirred for 3h. The completion of the successive reaction and the purity of the product were monitored with help of TLC. The dark brown solid product formed, filtered, washed with MeOH (3 x 20 mL) and dried in vacuum.

Yield= 68 %. m.p. = decompose above 300 ºC. Anal.Calcd for $C_{24}H_{54}N_{10}O_{13}NiSn_2Cl_6$: C, 24.03; H, 4.54; N, 11.68. Found: C, 24.02; H, 4.59; N, 11.67. IR (KBr) (ν_{max}/cm^{-1}): 3417 (O-H, NH_2,N-H, broad); 1539 (C=N); 1449 (δOCH, δCH_2, δCCH); 1401 (C-N); 526 (Ni-N); 422 (Sn-O); 338 (Sn-Cl); UV-vis. (1

x 10^{-3}M, H_2O, nm) 234, 276, 374, 615. ^{1}H NMR (400MHz, D_2O, δ): 8.56 (NH Imidazole, 2H); 7.34 (-CH Imidazole, 4H); 5.21 (NH GlcN, 4H); 4.71 (N-H tet, 2H); 4.26 - 2.80 (OH,H_2O,CH_2,CH GLcN-tet, 46H).^{13}C NMR (100 MHz, D_2O, δ): 146.77, 146.75, 144.53, 133.66, 133.61, 118.86 (6 C, imidazole rings); 74.21, 74.11, 73.38, 70.59, 69.52, 67.65, 62.13, 57.43, 54.79, 52.65, 49.92, 49.28 (12 C, GlcN); 48.92, 45.89, 44.60, 44.51, 43.22, 41.05 (6 C, amine). ^{119}Sn NMR (149.19 MHz, D_2O, δ): -615. ESI-MS (H_2O, +ve) expected (observed): 1168.5 (1168) $[C_{24}H_{54}N_{10}O_{13}NiSn_2Cl_5 + 4H]^+$.

Synthesis of tet(GLcN)$_2$Cu(Im)$_2$Sn$_2$

This complex was prepared by adopting the procedure given for **tet(GLcN)$_2$Ni(Im)$_2$Sn$_2$**, by using bis(imidazole)copper(II)chloride (0.270 g, 1mmol).

Yield= 74 %. m.p. = decompose at 290 ºC. Anal.Calcd for $C_{24}H_{54}N_{10}O_{13}CuSn_2Cl_6$: C, 23.93; H, 4.52; N, 11.63. Found: C, 23.96; H, 4.56; N, 11.62. IR(KBr) (ν_{max}/cm^{-1}): 3409 (O-H, NH_2, broad); 1537 (C=N); 1452 (δOCH, δCH_2, δCCH); 1420 (C-N); 540 (Cu-N); 460 (Sn-O); 337 (Sn-Cl); UV-vis. (1 x 10^{-3} M, H_2O, nm) 232, 270, 375, 650. ESI-MS (H_2O, +ve) expected (observed): 1172.98 (1173) $[C_{24}H_{54}N_{10}O_{13}CuSn_2Cl_5 + 4H]^+$.

Synthesis of tet(GLcN)$_2$Zn(Im)$_2$Sn$_2$

This was prepared by a procedure analogous to **tet(GLcN)$_2$Ni(Im)$_2$Sn$_2$**, by using bis(imidazole)zinc(II) chloride (0.272 g, 1mmol).

Yield= 77 %. m.p. = decompose at 295 ºC. Anal.Calcd for $C_{24}H_{52}N_{10}O_{12}ZnSn_2Cl_6$: C, 24.26; H, 4.41; N, 11.79. Found: C, 24.25; H, 4.77; N, 11.80. IR (KBr) (ν_{max} / cm^{-1}): 3414 (O-H, NH_2, broad); 1540 (C=N); 1450 (δOCH, δCH_2, δCCH); 1402 (C-N); 522

(Zn-N); 459 (Sn-O); 344 (Sn-Cl). UV-vis. (1 x 10^{-3}M, H_2O, nm) 230, 274, 345. ^{1}H NMR (400MHz, D_2O, δ): 8.59 (NH Imidazole, 2H); 7.37 (CH Imidazole, 4H); 5.22 (NH GlcN, 4H); 4.69 (N-H tet, 2H); 2.83-3.99 (OH, CH_2, CH GLcN-tet, 44H).^{13}C NMR (100 MHz, D_2O, δ): 145.00, 144.77, 141.18, 133.35, 1118.89, 115.06 (6 C, Imidazole); 74.22, 74.17, 73.36, 70.83, 69.56, 67.63, 62.88, 57.41, 54.38, 52.71, 50.10, 49.77 (12 C, GlcN); 48.87, 44.62, 43.25, 42.21, 41.07, 39.30 (6 C, amine). ^{119}Sn NMR (149.19 MHz, D_2O, δ): -619. ESI-MS: (H_2O, +ve): 1156.79 (1157) $[C_{24}H_{52}N_{10}O_{12}ZnSn_2Cl_5\,4H]^{+}$.

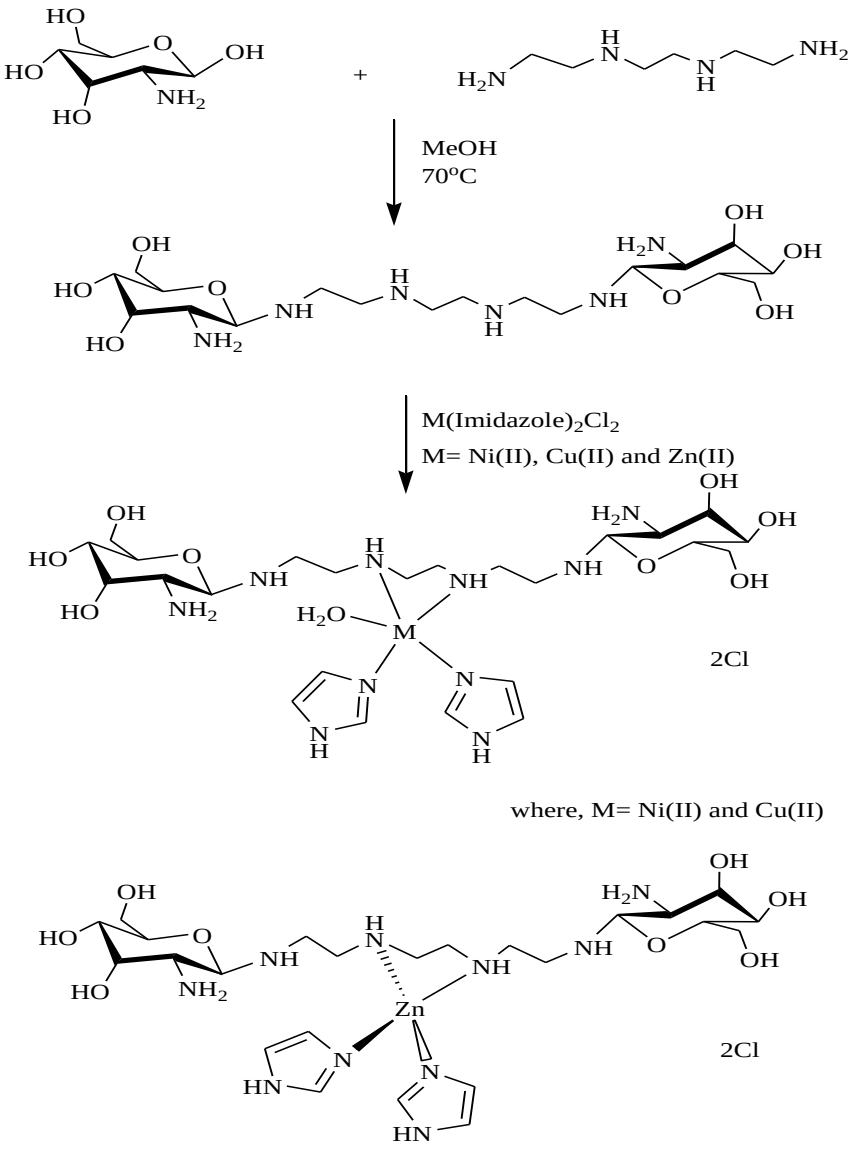

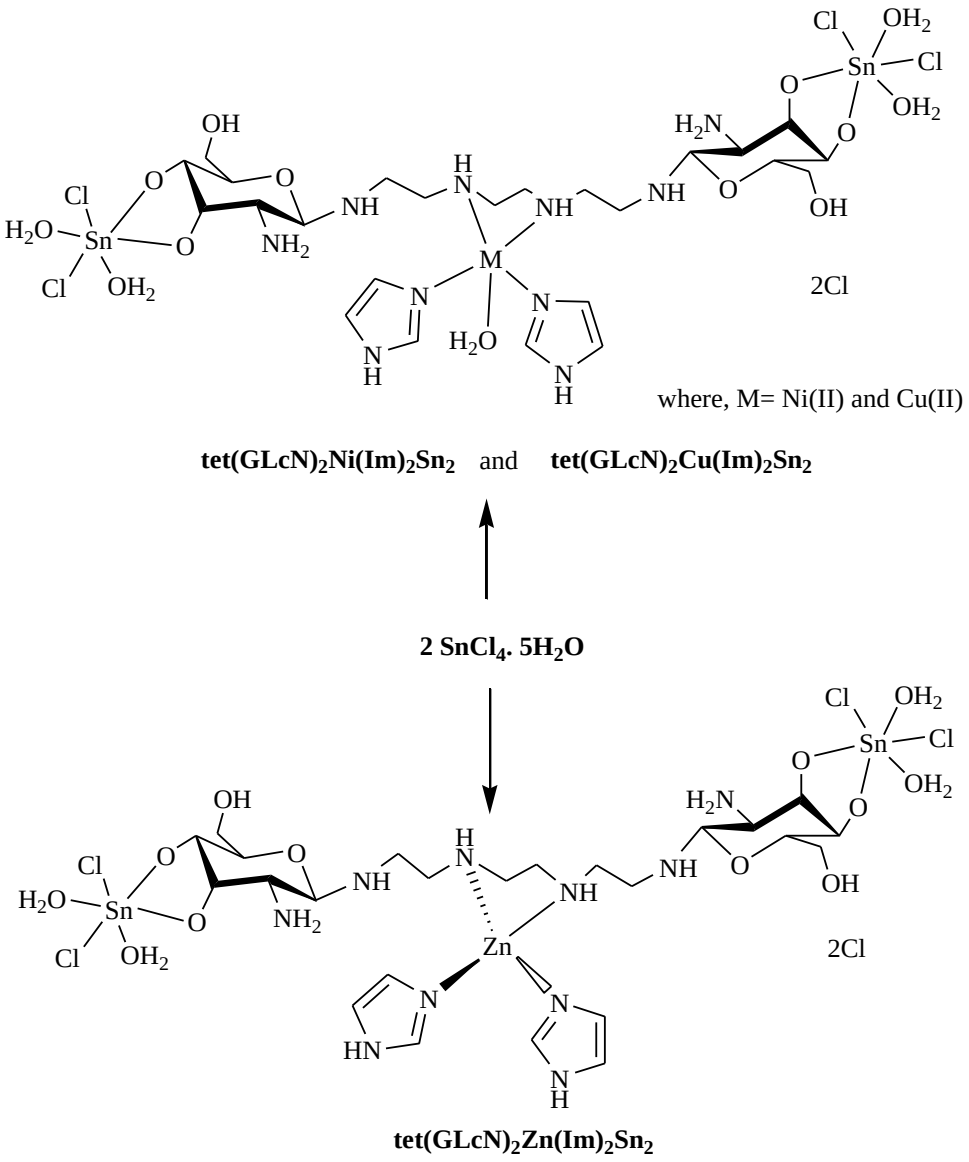

Scheme 1. *Syntheses of ligand, monometallic and heterobimetallic complexes (counter ions has been omitted)*

Results and Discussion

The synthesis of heterobimetallic complexes tet(GLcN)$_2$Ni(Im)$_2$Sn$_2$, tet(GLcN)$_2$Cu(Im)$_2$Sn$_2$, and tet(GLcN)$_2$Zn(Im)$_2$Sn$_2$ of 1,8-diamino-3,6-diazaoctane bridged N-glycoside, bis(imidazole)M(II)chloride (M= Ni, Cu and Zn) and $SnCl_4.5H_2O$, were achieved by one pot three step synthetic route in 1:1:2 stoichiometry (Scheme 1). The completion of the reaction at successive steps and

purity of the final product was monitored by thin layer chromatography. All the complexes are highly hygroscopic in nature and soluble in H_2O, DMF and DMSO. The molar conductivity (Λ_M) data for DMF solutions of all complexes observed in the range ~130-170 $\Omega^{-1}cm^2mol^{-1}$ indicated their 1:2 electrolytic natures. On the basis of spectral studies, the coordination geometry of the central metal ions viz. nickel(II) in complex tet$(GLcN)_2Ni(Im)_2Sn_2$ and copper(II) in complex tet$(GLcN)_2Cu(Im)_2Sn_2$ was square pyramidal, while in case of zinc(II) tet$(GLcN)_2Zn(Im)_2Sn_2$, it was found to be tetrahedral. ^{119}Sn NMR revealed the presence of two tin metal centers in the hexacoordinate environment. The X-ray powder diffraction (XRPD) confirmed the amorphous nature of all three complexes.

IR Spectroscopy

The IR spectra of all the complexes exhibit a merged broad band at ~3400 cm^{-1} characteristic for stretching vibrations of coordinated water molecule, hydrogen bonded O-H [214] and NH_2 groups of the sugar moiety. Due to the overlapping of bands, the individual stretching and bending frequencies for the above mentioned functional groups could not be assigned. The ν(C=N) vibrations of the imidazole rings lie in the range 1540-1537 cm^{-1} [215]. The strong characteristic bands appearing between 1458-1402 cm^{-1} were attributed to δ(OCH, CH_2, CCH), while the bands at 1092-1034 cm^{-1} were assigned to ν(CO, CC). The occurrence of broad bands for all the vibrational modes rendered the individual assignments difficult [216]. The far IR spectra of the complexes exhibited non ligand absorption bands at 540-522 cm^{-1}, 462-459 cm^{-1}, and 344-337 cm^{-1}, due to ν(M-N), ν(Sn-O), and ν(Sn-Cl) vibrations [217,218], respectively which ascertained the chelation of tin and transition metal ions

to the N-GlcN through oxygen atom and NH of the linker 1,8-diamino-3,6-diazaoctane, respectively.

NMR spectroscopy

The ^{1}H, ^{13}C and ^{119}Sn NMR spectra of the ligand, complexes tet$(GLcN)_2Ni(Im)_2Sn_2$ and tet$(GLcN)_2Zn(Im)_2Sn_2$ were recorded in D_2O. The ^{1}H NMR spectrum of the ligand exhibits the superposed multiplet peaks in the range 3.87 - 2.78 ppm assigned to the sugar OH, CH_2, CH and the amine NH and CH_2. The signal at 5.20 ppm was attributed to NH_2 protons of glucosamine moiety, respectively. The ^{1}H NMR spectra of complexes tet$(GLcN)_2Ni(Im)_2Sn_2$ and tet$(GLcN)_2Zn(Im)_2Sn_2$ revealed signals at δ = 4.26 - 2.83 ppm and 3.99 - 2.80 ppm respectively, attributed to the skeletal protons of the D-GlcN and CH_2 protons of linker 1,8-diamino-3,6-diazaoctane. Due to the resonances arising from the different types of protons in the same region, the proton signals could not be assigned individually [211, 219]. The broad envelopes at δ 4.71 and 5.21 ppm were assigned to NH and NH_2 protons of the linker moiety and D-GlcN, respectively. The aromatic protons of the imidazole ring were observed at 7.37 - 7.34 ppm, while NH protons appeared in the range 8.59 - 8.56 ppm [220].

The ^{13}C NMR spectrum of the ligand, displays the signals of 6 carbons of the linker 1,8-diamino-3,6-diazaoctane in the range 49.68 – 45.59 ppm, and 74.43 - 49.86 ppm for the 12 carbons of D-glucosamine. The ^{13}C NMR spectra of the tet$(GLcN)_2Ni(Im)_2Sn_2$ and tet$(GLcN)_2Zn(Im)_2Sn_2$ complexes displayed the signals at 48.92 – 41.05 and 48.87 - 39.30 ppm, respectively assigned to the six carbons of the linker amine. The peaks for the twelve distinct carbon atoms of the D-glucosamine were observed in the range of 74.21 - 49.28 ppm for complex 1 and 74.22 - 49.37 ppm for tet$(GLcN)_2Zn(Im)_2Sn_2$ displayed, with the downfield carbon atom signals

corresponding to (C(1)) and (C(1′)) i.e. the anomeric carbons of the sugar moiety. Other carbons were observed upfield in the order of (C(5)), (C(5′)),(C(3)), (C(3′)), (C(6)), (C(6′)), (C(4)), (C(4′)), (C(2)) (C(2′)) according to the literature reports [62]. Additionally the aromatic carbons of imidazole appeared in the range 146.77 - 118.86 ppm and 148.21 - 115.06 ppm (Figure 38). The geometry of tin (IV) metal ions in tet$(GLcN)_2Ni(Im)_2Sn_2$ and tet$(GLcN)_2Zn(Im)_2Sn_2$ was validated by ^{119}Sn NMR spectroscopy. It is known that ^{119}Sn chemical shift δ (^{119}Sn) is sensitive towards the coordination sphere around the tin atom. ^{119}Sn NMR spectra of both tet$(GLcN)_2Ni(Im)_2Sn_2$ and tet$(GLcN)_2Zn(Im)_2Sn_2$ showed a single peak for two tin metal atoms at -585 ppm and -619 ppm, respectively due to the same environment around the tin centers [221,222]. These chemical shift values are in close agreement with the octahedral environment around the tin atoms in the heterobimetallic complexes previously reported by our group [43,158].

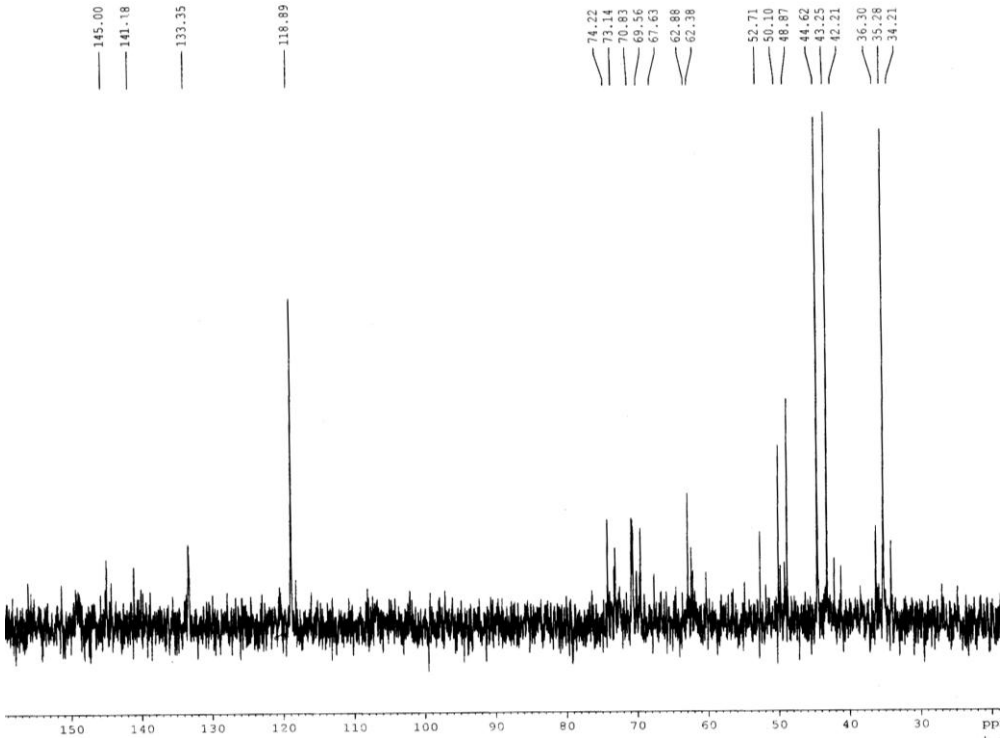

Figure 38. *^{13}C NMR spectrum of the complex tet$(GLcN)_2Zn(Im)_2Sn_2$ complex (**3**) in D_2O.*

ESR spectroscopy

The liquid state X-band EPR spectrum of tet$(GLcN)_2Cu(Im)_2Sn_2$ in DMSO acquired at room temperature has been found to be anisotropic exhibiting two peaks, $g_{\|}$ = 2.21 and $g_{\perp}$= 2.04 (Figure 39). The value $g_{\|} > g_{\perp} \sim g_e$ (g_e =2.0023) is indicative of a $\{d_{x^2-y^2}\}^1$ or $\{d_{z^2}\}^1$ ground state of the Cu(II) ion, in a square pyramidal geometry [223]. For a Cu(II) complex, $g_{\|}$ is a parameter sensitive enough to indicate covalence. For a covalent complex, $g_{\|}$ is < 2.3 and for an ionic environment, $g_{\|}$ = 2.3 or more. In the present complex $g_{\|}$ < 2.3 indicates an appreciable metal-ligand covalent character [224]

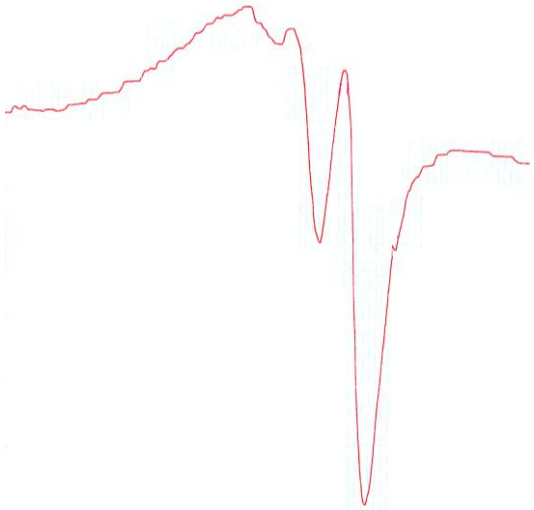

Figure 39*. ESR spectrum of the complex tet$(GLcN)_2Cu(Im)_2Sn_2$ at LNT.*

Electronic spectra

The electronic absorption spectra of the all complexes were carried out in the range 190-1100 nm. The electronic spectrum of tet$(GLcN)_2Ni(Im)_2Sn_2$ displayed, spin allowed transition at 615 nm assigned to $^3B_1(F) \rightarrow {}^3E(F)$ transition suggesting a pentacoordinate geometry around Ni(II) metal ion [225]. The spectrum also exhibited LMCT transitions at 374 and 276 nm inaddition to intraligand band at 234 nm. The

UV/vis spectrum of tet(GLcN)$_2$Cu(Im)$_2$Sn$_2$ and revealed a prominent band at 650 nm attributed to d_{xz}, $d_{yz} \rightarrow d_{x^2-y^2}$ ligand field transition, followed by a shoulder at 375 nm and two strong bands at 270 and 232 nm in the UV region assigned to the ligand to metal charge transfer (LMCT) and intraligand charge transfer (IL) bands, respectively. These results are typical of square pyramidal geometry around Cu(II) ion [226]. This is in accordance with the EPR studies. Similarly, the absorption spectrum of complex tet(GLcN)$_2$Zn(Im)$_2$Sn$_2$ revealed bands at 345, 274 and 230 nm due to LMCT and intraligand transitions, respectively.

X-ray diffraction analysis

To obtain further evidence about the structures of the metal complexes, X-ray powder diffraction was performed (Figure 40). The XRPD patterns ascertained amorphous nature of the complexes tet(GLcN)$_2$Ni(Im)$_2$Sn$_2$, tet(GLcN)$_2$Cu(Im)$_2$Sn$_2$, and tet(GLcN)$_2$Zn(Im)$_2$Sn$_2$.

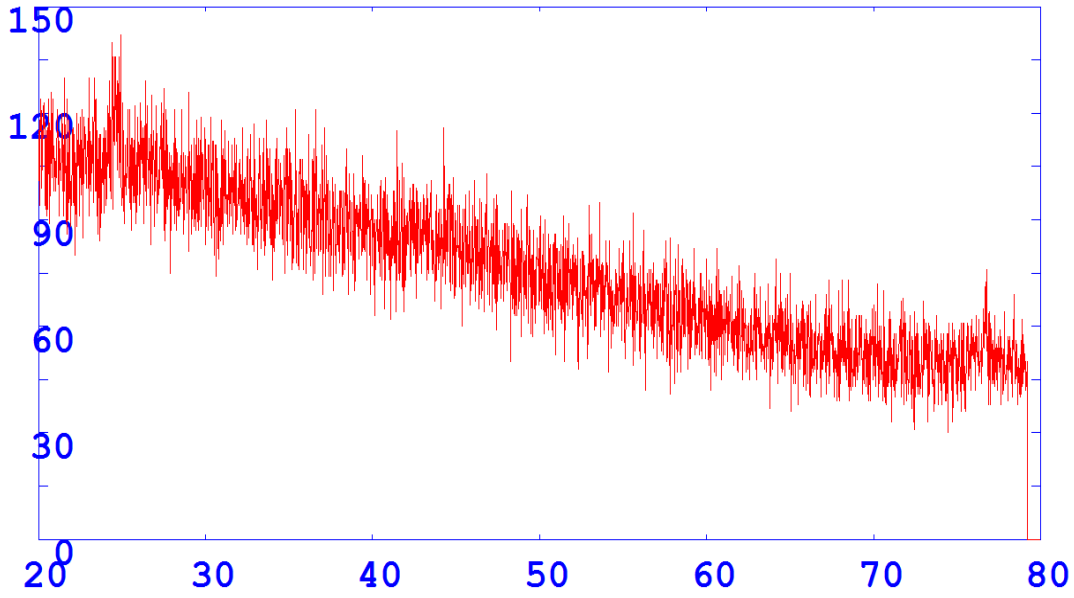

Figure 40. *X-ray powder diffraction patterns of tet(GLcN)$_2$Zn(Im)$_2$Sn$_2$.*

Biological studies

The binding studies of tet$(GLcN)_2Cu(Im)_2Sn_2$ and tet$(GLcN)_2Zn(Im)_2Sn_2$ with CT DNA were carried out by using absorption, emission spectroscopic titrations and cyclic voltammetry. To elucidate the specific binding site the absorption titrations were carried out with nucleotides viz., 5'-AMP, 5'-CMP, 5'-GMP and 5'-TMP. The results obtained were further confirmed by ^{1}H, ^{119}Sn and ^{31}P NMR experiments by carrying out the interaction studies of tet$(GLcN)_2Cu(Im)_2Sn_2$ and tet$(GLcN)_2Zn(Im)_2Sn_2$ with 5'-GMP and 5'-TMP, respectively.

Absorption Spectral Studies

The interaction between complexes tet$(GLcN)_2Cu(Im)_2Sn_2$ and tet$(GLcN)_2Zn(Im)_2Sn_2$ with CT DNA, was carried out by employing electronic absorption spectroscopy. Both tet$(GLcN)_2Cu(Im)_2Sn_2$ and tet$(GLcN)_2Zn(Im)_2Sn_2$ complexes exhibited intense absorption bands at 230-232 and 270-274 nm attributed to intraligand transitions. A fixed concentration ($0.16x\ 10^{-4}$ M) of tet$(GLcN)_2Cu(Im)_2Sn_2$ and tet$(GLcN)_2Zn(Im)_2Sn_2$ was titrated with increasing amounts of CT DNA ($0\text{-}33.3 \times 10^{-6}$M). An increase in absorption intensity 'hyperchromicity' was observed at the intraligand bands as depicted in the (Figure. 41a,b). Since tet$(GLcN)_2Cu(Im)_2Sn_2$ and tet$(GLcN)_2Zn(Im)_2Sn_2$ possess heterobimetallic core Cu^{II}-Sn_2^{IV} and Zn^{II}-Sn_2^{IV}, respectively, they are expected to exhibit a unique dual mode of preferential binding with CT DNA. Furthermore, the complexes are appended with the glycoside unit which features novelty not only from the structural point of view, but also provides molecular recognition at the specific site; it drives the complexes towards the phosphate sugar backbone of DNA double helix which is clearly evidenced by the substantial 'hyperchromic effect' (32% and

27% for tet$(GLcN)_2Cu(Im)_2Sn_2$ and tet$(GLcN)_2Zn(Im)_2Sn_2$, respectively). The Sn(IV) ions (non-transition metal ions) of the complexes would exhibit preference for the phosphate sugar backbone of DNA double helix [43,158,227] via electrostatic interaction presumably reinstated by coordinate covalent binding tendency of the central transition metal ion Cu(II) / Zn(II) towards the heteroatom of the nucleobase pairs [158] which is indicated by the bathochromic shift *ca*. 3-4 nm in their absorbance maxima. Literature supports that the copper ion specifically bind to the N7 of guanine and zinc ion to N3 of the thymine residue of DNA and cause strand breakage [228,229]. The more significant hyperchromism observed at 260 - 270 nm absorption band is indicative of strong electrostatic interaction of Sn(IV) ions towards the phosphate ends of the DNA. Nevertheless, DNA double helix possesses many hydrogen bonding sites positioned on the edges of the DNA bases, it is quite amenable that the coordinated –NH– groups and –OH groups of the ligand could participate in hydrogen bonding with the DNA base pairs [226-230].

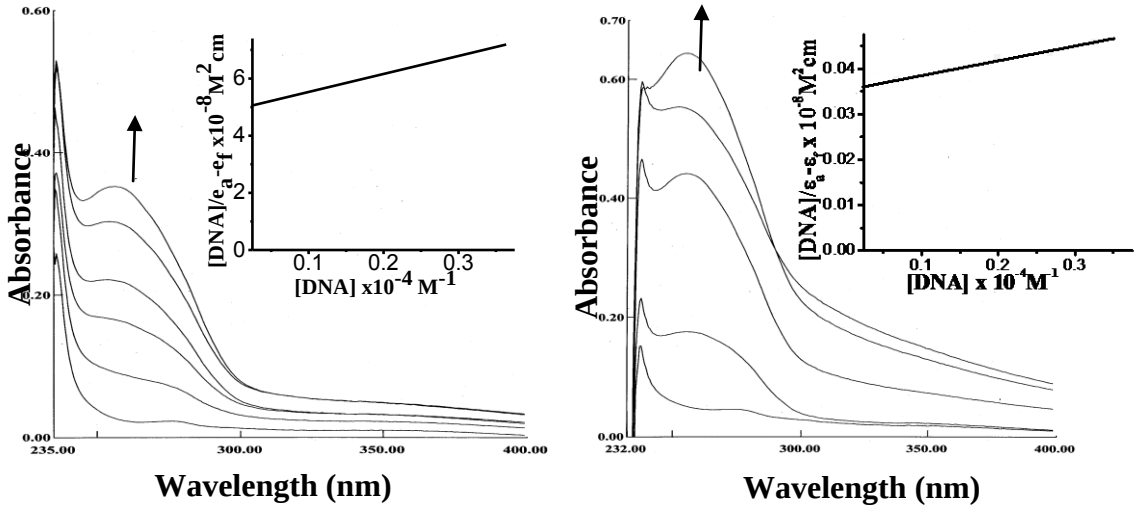

Figure 41. *Variation of UV-Vis absorption (a) for complex tet$(GLcN)_2Cu(Im)_2Sn_2$ and (b) for complex tet$(GLcN)_2Zn(Im)_2Sn_2$, with increase in the concentration of CT DNA in buffer (5mM Tris–HCl/50 mM NaCl, pH= 7.2) at room temperature {[DNA] (0.066-0.333)10^{-4} M}.*

To compare quantitatively the binding strength of tet$(GLcN)_2Cu(Im)_2Sn_2$ and tet$(GLcN)_2Zn(Im)_2Sn_2$ towards CT DNA, the intrinsic binding constants K_b were evaluated and values were found to be 2.25 x 10^4 M^{-1} and 0.98 x 10^4 M^{-1}, respectively. The K_b values are much lower in magnitude in comparison to the classical intercalators viz; EthBr-DNA (K_b = 1 x 10^6 M^{-1}) [231]. So, these observations support the contention that tet$(GLcN)_2Cu(Im)_2Sn_2$ and tet$(GLcN)_2Zn(Im)_2Sn_2$ exhibit an efficient DNA binding propensity by electrostatic and coordination mode of interaction to heterocyclic bases of the DNA double helix. Furthermore, the site selectivity and possible mode of binding was authenticated by carrying out the interaction of tet$(GLcN)_2Cu(Im)_2Sn_2$ and tet$(GLcN)_2Zn(Im)_2Sn_2$ with nucleotides viz 5'-GMP, 5'-TMP, 5'-AMP and 5'-CMP using UV-vis absorption spectroscopy.

Interaction of tet$(GLcN)_2Cu(Im)_2Sn_2$ and tet$(GLcN)_2Zn(Im)_2Sn_2$ with nucleotides

Literature reveals that interaction of pyrimidines and purines with Cu(II) and Zn(II) ions occur mainly via N7, N3 and N1 coordinating sites while O6 position is favored in other early transition metal ions [226-229]. Interaction studies of tet$(GLcN)_2Cu(Im)_2Sn_2$ and tet$(GLcN)_2Zn(Im)_2Sn_2$ with the nucleotides viz, 5'-AMP, 5'-CMP, 5'-GMP and 5'-TMP by UV-vis absorption titrations have been carried out by a similar method as described for titration of tet$(GLcN)_2Cu(Im)_2Sn_2$ and tet$(GLcN)_2Zn(Im)_2Sn_2$ with CT DNA. The absorption spectral traces of tet$(GLcN)_2Cu(Im)_2Sn_2$ and tet$(GLcN)_2Zn(Im)_2Sn_2$ (Figure 42(a-d)) in presence of increasing concentration of nucleotides exhibited hyperchromism implying that tet$(GLcN)_2Cu(Im)_2Sn_2$ and tet$(GLcN)_2Zn(Im)_2Sn_2$ binds electrostatically to phosphate oxygen atoms in addition to covalent interaction with the nucleobases. In order to

compare their binding affinity, the intrinsic binding constants K_b of the complexes with nucleotides were calculated.

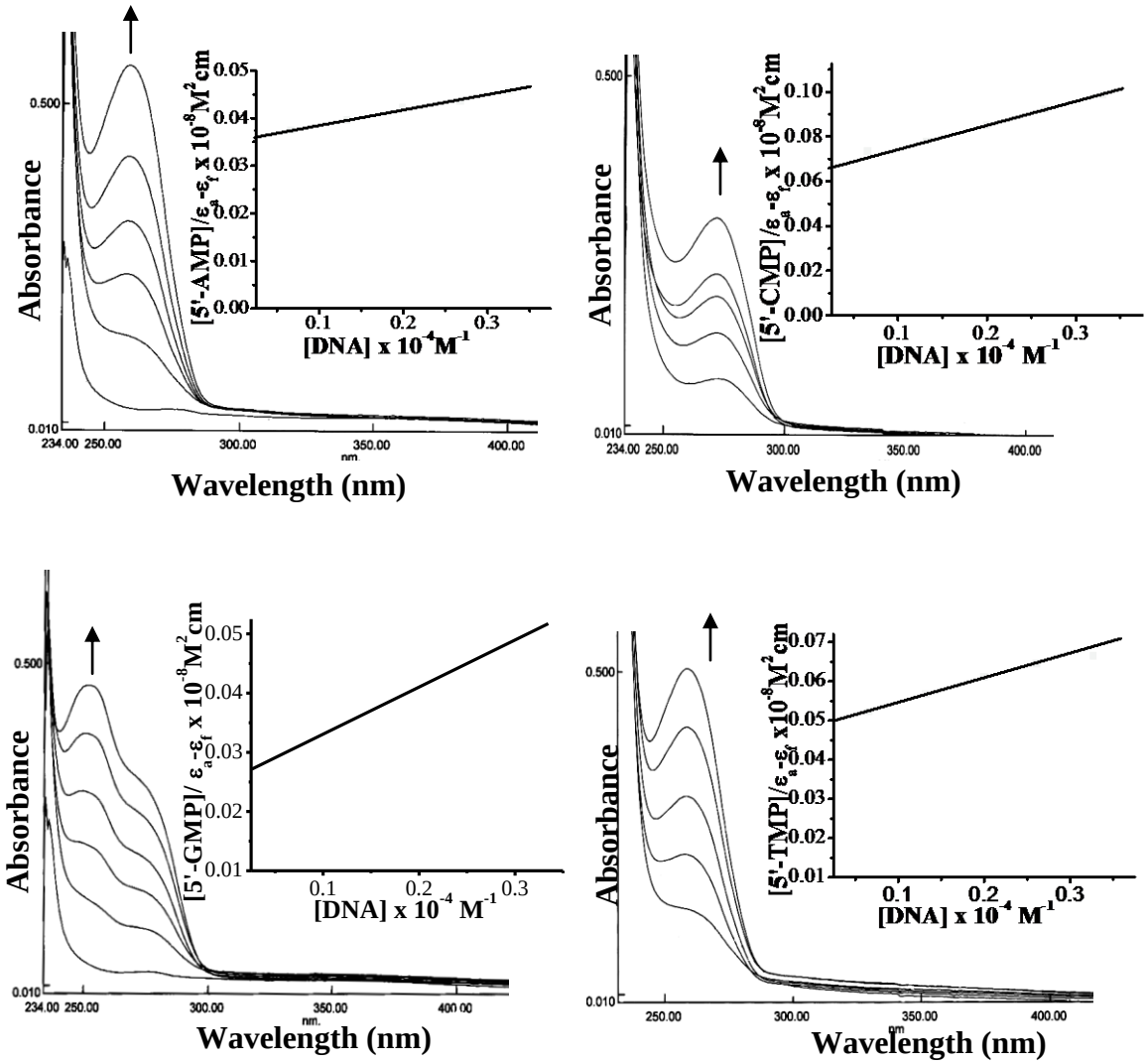

***Figure 42**. Absorption spectral traces of complex tet(GLcN)$_2$Cu(Im)$_2$Sn$_2$ with (a) 5'-AMP, (b) 5'-CMP (c) 5'-GMP and (d) 5'-TMP in buffer (5mM Tris–HCl/50 mM NaCl, pH= 7.2) at room temperature {[Nucleotide] (0.066-0.333)10^{-4} M}.*

The binding constant values as given in the table 3, reveal that tet(GLcN)$_2$Cu(Im)$_2$Sn$_2$ show higher binding affinity towards 5'-GMP while tet(GLcN)$_2$Zn(Im)$_2$Sn$_2$ to 5'-TMP. These results are consistent with the observed hyperchromic effect of tet(GLcN)$_2$Cu(Im)$_2$Sn$_2$ and tet(GLcN)$_2$Zn(Im)$_2$Sn$_2$ bound to CT DNA. Further

confirmation of binding mode was done by carrying out interaction studies of complex tet$(GLcN)_2Cu(Im)_2Sn_2$ and tet$(GLcN)_2Zn(Im)_2Sn_2$ with 5'-GMP and 5'-TMP, respectively by ^{1}H, ^{119}Sn and ^{31}P NMR experiments.

***Table 3**: The binding constant (K_b) values of complexes **2** and **3** with the nucleotides (mean standard deviation of ± 0.2)*

Complex	**5'-AMP** (10^4 M^{-1})	**5'-CMP** (10^4 M^{-1})	**5'-GMP** (10^4 M^{-1})	**5'-TMP** (10^4 M^{-1})
tet$(GLcN)_2Cu(Im)_2Sn_2$	1.30	1.75	3.22	1.22
tet$(GLcN)_2Zn(Im)_2Sn_2$	1.04	0.48	0.66	2.00

NMR spectroscopic studies of tet$(GLcN)_2Cu(Im)_2Sn_2$ and tet$(GLcN)_2Zn(Im)_2Sn_2$ with 5'-GMP and 5'-TMP, respectively

To further investigate the selective recognition and the binding mode exhibited by tet$(GLcN)_2Cu(Im)_2Sn_2$ and tet$(GLcN)_2Zn(Im)_2Sn_2$ complexes towards 5'-GMP and 5'-TMP, respectively, ^{1}H, ^{31}P and ^{119}Sn NMR experiments were performed (Figure 43 and 44). The ^{1}H NMR spectrum of 5'-GMP in D_2O in presence of tet$(GLcN)_2Cu(Im)_2Sn_2$ displays H8 proton adjacent to N7 atom of guanine at 8.56 ppm, downfielded by 0.51 ppm with respect to 8.05 ppm observed in free 5'-GMP NMR spectrum. The downfield shift results due to the desheilding of H8 proton by coordinate bond formation of Cu(II) ions of complex tet$(GLcN)_2Cu(Im)_2Sn_2$ with the neighboring N7 atom of guanine base. To confirm the involvement of electrostatic interaction, ^{31}P and ^{119}Sn NMR spectra of the free 5'-GMP and tet$(GLcN)_2Cu(Im)_2Sn_2$

+ 5'-GMP were recorded. The ^{31}P NMR spectrum of tet$(GLcN)_2Cu(Im)_2Sn_2$ + 5'-GMP showed a shift from δ = 3.59 ppm to -0.77 ppm with the decrease in the intensity of signal associated with the phosphate group [232]. Furthermore, in the ^{119}Sn NMR spectrum of tet$(GLcN)_2Cu(Im)_2Sn_2$ + 5'-GMP the peak corresponding to two tin metal ions shifted to δ = -615 ppm from δ = -585 ppm. Thus, our experiments clearly confirm the dual mode of binding of tet$(GLcN)_2Cu(Im)_2Sn_2$ with 5'-GMP viz, the coordinative interactions between Cu(II) ions and N7 of 5'-GMP and the electrostatic mode of interaction between phosphate groups with the tin centers.

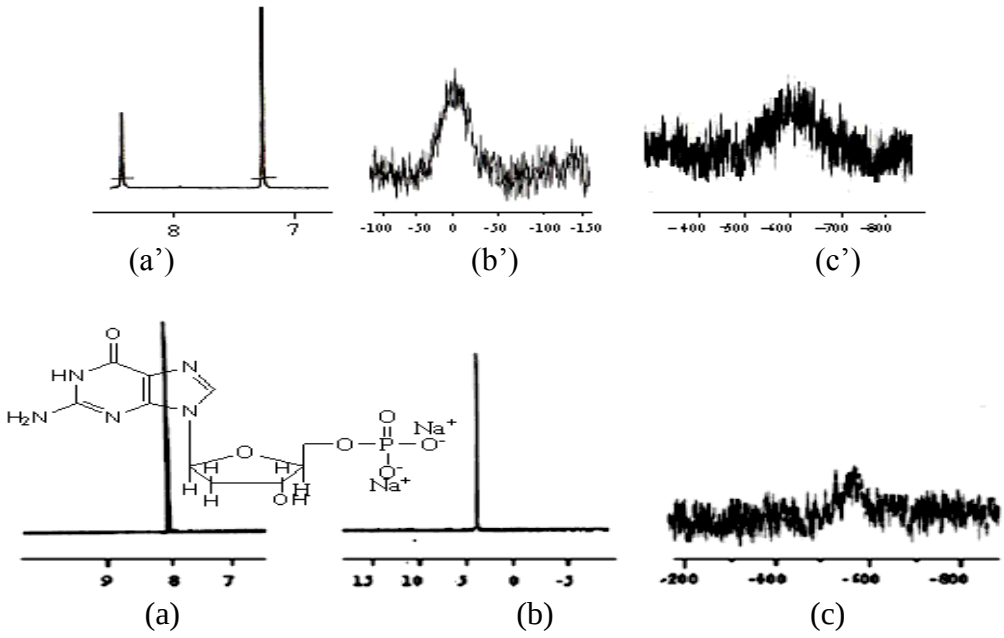

Figure 43. (a) ^1H NMR spectrum of free 5'-GMP, (b) ^{31}P NMR spectrum of free 5'-GMP, (c) ^{119}Sn NMR spectrum of tet$(GLcN)_2Cu(Im)_2Sn_2$ complex (a') ^1H NMR spectrum of tet$(GLcN)_2Cu(Im)_2Sn_2$+5'-GMP, (b') ^{31}P NMR spectrum of tet$(GLcN)_2Cu(Im)_2Sn_2$+5'-GMP, (c') ^{119}Sn NMR spectrum of tet$(GLcN)_2Cu(Im)_2Sn_2$ complex +5'-GMP in D_2O at room temperatures.

In an analogous way, when tet$(GLcN)_2Zn(Im)_2Sn_2$ was treated with the 5'-TMP, the ^1H NMR spectrum showed no significant shift of N3 proton, as compared to that of

free 5'-TMP. Consequently, the N3 coordination was ruled out. Nevertheless, the possibility of interaction of tet(GLcN)$_2$Zn(Im)$_2$Sn$_2$ with oxygen of carbonyl groups of thymine base by hydrogen bonding cannot be neglected. However, the ^{31}P and ^{119}Sn NMR spectral information strongly supports the electrostatic binding of phosphate group with Sn(IV) atoms. The ^{31}P NMR spectrum showed slight shift with decrease in intensity of the peak to δ = -0.04 ppm in tet(GLcN)$_2$Zn(Im)$_2$Sn$_2$ + 5'-TMP from δ = 2.5 ppm for 5'-TMP alone. The^{119}Sn NMR spectrum of the tet(GLcN)$_2$Zn(Im)$_2$Sn$_2$ + 5'-TMP exhibited a signal at δ = -630 in comparison to δ = -619 ppm for untreated tet(GLcN)$_2$Zn(Im)$_2$Sn$_2$ complex with apparent line broadening, thus corroborating with an electrostatic mode of interaction of Sn(IV) ions of tet(GLcN)$_2$Zn(Im)$_2$Sn$_2$ complex to the phosphate ends of the 5'-TMP.

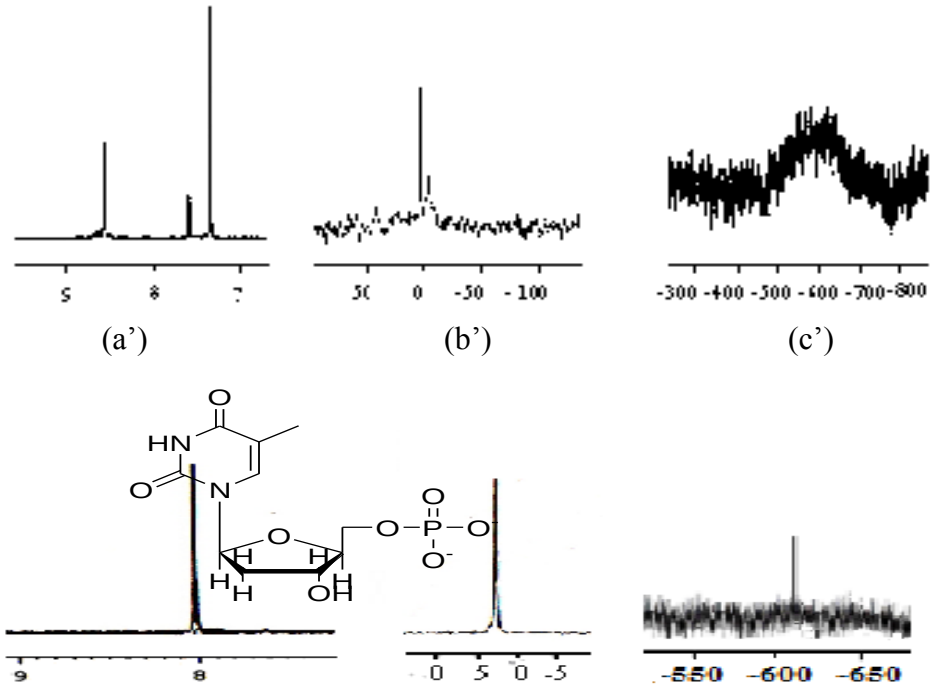

Figure 44. *(a) ^{1}H NMR spectrum of free 5'-TMP, (b) ^{31}P NMR spectrum of free 5'-TMP, (c) ^{119}Sn NMR spectrum of tet(GLcN)$_2$Zn(Im)$_2$Sn$_2$ complex. (a') ^{1}H NMR spectrum of tet(GLcN)$_2$Zn(Im)$_2$Sn$_2$+5'-TMP, (b') ^{31}P NMR spectrum of tet(GLcN)$_2$Zn(Im)$_2$Sn$_2$ +5'-TMP, (c') ^{119}Sn NMR spectrum of complex tet(GLcN)$_2$Zn(Im)$_2$Sn$_2$ +5'-TMP,in D$_2$O at room temperatures.*

Steady-state emission titration

Both tet$(GLcN)_2Cu(Im)_2Sn_2$ and tet$(GLcN)_2Zn(Im)_2Sn_2$ complexes exhibited emission bands at 545 nm when excited at 260 nm. In the absence of CT DNA, tet$(GLcN)_2Cu(Im)_2Sn_2$ and tet$(GLcN)_2Zn(Im)_2Sn_2$ emit weak luminescence in 5mM Tris-HCl/50 mM NaCl buffer at ambient temperature. Upon the addition of CT DNA the emission intensity of tet$(GLcN)_2Cu(Im)_2Sn_2$ and tet$(GLcN)_2Zn(Im)_2Sn_2$ complexes increased as shown in figure 45(a,b).

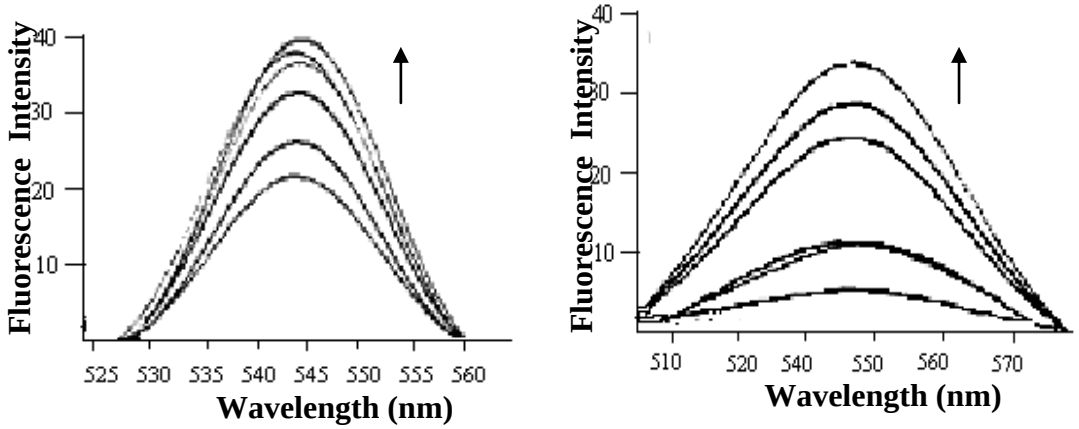

***Figure 45**. Emission spectra of (a) tet$(GLcN)_2Cu(Im)_2Sn_2$ complex and (b) tet$(GLcN)_2Zn(Im)_2Sn_2$ complex, in the absence and in presence of CT DNA in buffer (5mM Tris –HCl/50mM NaCl, pH= 7.2) at room temperature.*

The hydrophobic molecular structure of CT DNA could be responsible for enhancing the fluorescence quantum yield of complexes, leading to the higher fluorescence intensity with the increase in concentration of the CT DNA. In addition, energy transfer from CT DNA to metal complexes could also induce fluorescence enhancement [233]. The CT DNA binding constant of the tet$(GLcN)_2Cu(Im)_2Sn_2$ and tet$(GLcN)_2Zn(Im)_2Sn_2$ complexes were obtained from Scatchard equation with mean standard deviations (± 0.3) and followed the order, tet$(GLcN)_2Cu(Im)_2Sn_2$ (K = 3.4

$x10^4$ M^{-1}) > tet$(GLcN)_2Zn(Im)_2Sn_2$ (K = 2.1 $x10^4$ M^{-1}). These results are consistent with the findings obtained from UV-vis spectral studies.

Ethidium Bromide Displacement Assay

To further investigate the mode of binding of the tet$(GLcN)_2Cu(Im)_2Sn_2$ and tet$(GLcN)_2Zn(Im)_2Sn_2$ complexes, the ethidium bromide displacement assay was carried out [234].

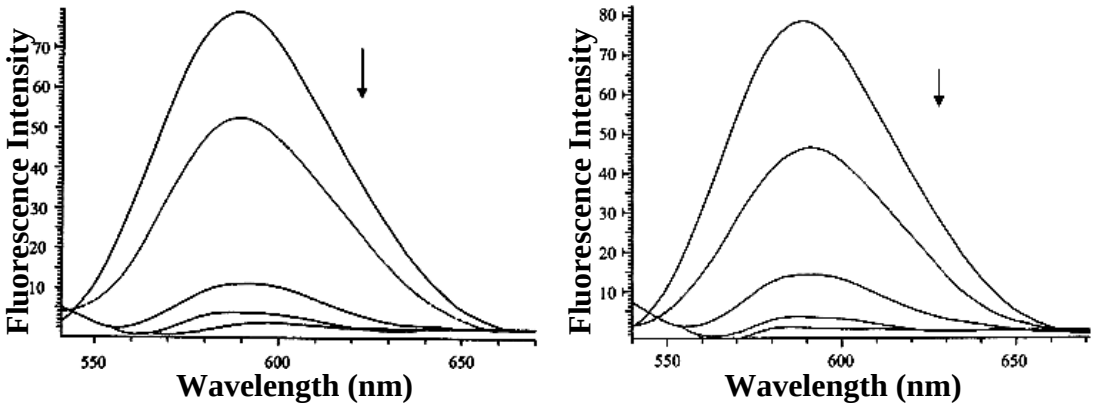

Figure 46*. Fluorescence quenching spectra of CT DNA bound ethidium bromide in the presence of (a) tet$(GLcN)_2Cu(Im)_2Sn_2$ complex and (b) tet$(GLcN)_2Zn(Im)_2Sn_2$ complex, at different concentrations in buffer (5mM Tris –HCl/ 50 mM NaCl, pH= 7.2) at room temperature*.

The extent of quenching of the fluorescence of EthBr bound to DNA would reflect the extent of DNA binding of tet$(GLcN)_2Cu(Im)_2Sn_2$ and tet$(GLcN)_2Zn(Im)_2Sn_2$. On addition of complexes tet$(GLcN)_2Cu(Im)_2Sn_2$ and tet$(GLcN)_2Zn(Im)_2Sn_2$, to CT DNA pretreated with EthBr ([DNA]/[EthBr] = 1) the decrease in emission intensity was observed. The emission intensity in the absence and in presence of tet$(GLcN)_2Cu(Im)_2Sn_2$ and tet$(GLcN)_2Zn(Im)_2Sn_2$ with EthBr-DNA are depicted in figure 46(a,b). As there is incomplete quenching of the EthBr-induced emission intensity, the intercalative binding mode for tet$(GLcN)_2Cu(Im)_2Sn_2$ and

tet$(GLcN)_2Zn(Im)_2Sn_2$ was ruled out. Further, the quenching extents of tet$(GLcN)_2Cu(Im)_2Sn_2$ and tet$(GLcN)_2Zn(Im)_2Sn_2$ were quantitatively evaluated. The K_{sr} values i,e., quenching constants for tet$(GLcN)_2Cu(Im)_2Sn_2$ and tet$(GLcN)_2Zn(Im)_2Sn_2$ were found to be 2.6 x 10^5 M^{-1} and 1.76 x 10^5 M^{-1} , respectively. The higher value of K_{sr} for tet$(GLcN)_2Cu(Im)_2Sn_2$ was attributed to covalent binding with heterocyclic nitrogen atom of nucleobase.

Electrochemical Studies

Electrochemical techniques provide a useful complement to the other related biophysical techniques to study the interaction of the redox active molecules with the biomolecules [235]. The cyclic voltammogram of tet$(GLcN)_2Cu(Im)_2Sn_2$ and tet$(GLcN)_2Zn(Im)_2Sn_2$ in the absence and in presence of CT DNA were recorded in aqueous solutions with 0.4 M KNO_3 as a supporting electrolyte (Figure 47). The cyclic voltammograms of tet$(GLcN)_2Cu(Im)_2Sn_2$ and tet$(GLcN)_2Zn(Im)_2Sn_2$ exhibited ratio of the peak currents lower than 1 attributed to quasireversible one electron redox process involving M^n/M^{n-1} couple. The cyclic voltammogram of tet$(GLcN)_2Cu(Im)_2Sn_2$ showed reduction of Cu^{II}/Cu^{I} at a cathodic peak potential E_{pc} (–0.368 V) while oxidation was observed at anodic peak potential (–0.273V). The separation of the anodic and cathodic peak potential ΔE_p = -0.095 V and I_{pa}/I_{pc} ratio = 0.483. tet$(GLcN)_2Zn(Im)_2Sn_2$ complex featured reduction of Zn^{II}/Zn^{I} form at a cathodic peak potential (E_{pc}) of –0.368 V and anodic peak (E_{pa}) at –0.254 V and the separation between anodic and cathodic peak potential were ΔE_p = - 0.114 V and I_{pa}/I_{pc} ratio = 0.38. The addition of CT DNA to the tet$(GLcN)_2Cu(Im)_2Sn_2$ and tet$(GLcN)_2Zn(Im)_2Sn_2$ complex results in a significant reduction in respective peak

potentials as well as in the cathodic and anodic peak currents which can be attributed to slow diffusion of an equilibrium mixture of the free and DNA bound complexes to the electrode surface [236,237].

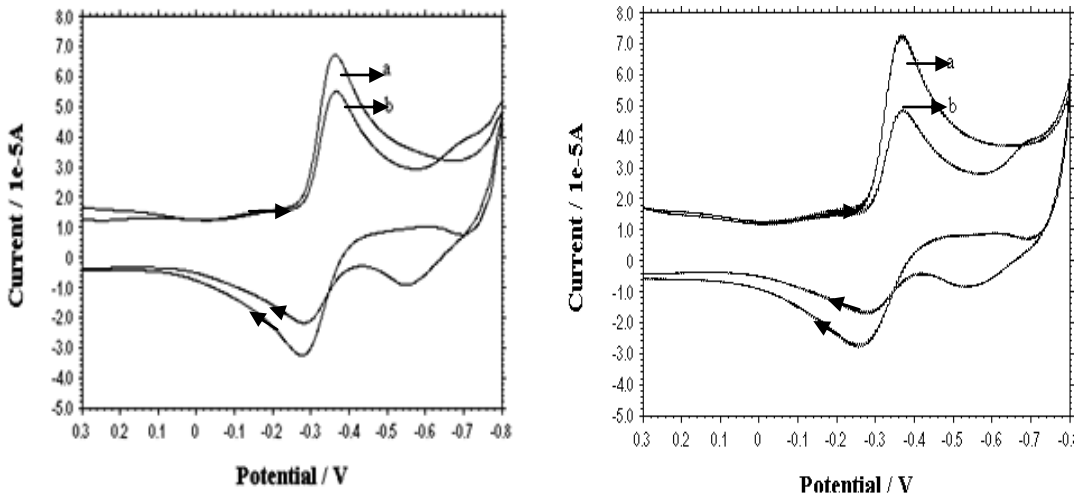

Figure 47*. Cyclic voltammogram of complex tet(GLcN)$_2$Cu(Im)$_2$Sn$_2$ and tet(GLcN)$_2$Zn(Im)$_2$Sn$_2$ respectively at scan rate 0.3 Vs^{-1}(a) in the absence and (b) in presence of CT DNA at room temperature under nitrogen atmosphere.*

Table 4: *Voltammetric behaviour of tet(GLcN)$_2$Cu(Im)$_2$Sn$_2$ and tet(GLcN)$_2$Cu(Im)$_2$Sn$_2$ complexes, in the absence and in presence of CT DNA.*

Complex	**E_{pc} (V)**	**E_{pa} (V)**	**$E_{1/2}$ (V)**	**ΔE (V)**	**I_{pa}/I_{pc}**
tet(GLcN)$_2$Cu(Im)$_2$Sn$_2$	-0.368	-0.273	-0.321	0.095	0.483
tet(GLcN)$_2$Cu(Im)$_2$Sn$_2$ + CT DNA	-0.368	-0.286	-0.320	0.082	0.392
tet(GLcN)$_2$Zn(Im)$_2$Sn$_2$	-0.368	-0.254	-0.311	0.114	0.385
tet(GLcN)$_2$Zn(Im)$_2$Sn$_2$ + CT DNA	-0.368	-0.279	-0.324	0.089	0.329

However, the larger shift in ΔE_p, $E_{1/2}$ and I_{pa}/I_{pc} values observed for tet(GLcN)$_2$Cu(Im)$_2$Sn$_2$ than tet(GLcN)$_2$Zn(Im)$_2$Sn$_2$ suggests that

tet$(GLcN)_2Cu(Im)_2Sn_2$ binds more strongly to CT DNA as compared to tet$(GLcN)_2Cu(Im)_2Sn_2$ and tet$(GLcN)_2Zn(Im)_2Sn_2$. The electrochemical data for tet$(GLcN)_2Cu(Im)_2Sn_2$ and tet$(GLcN)_2Zn(Im)_2Sn_2$ with CT DNA is given in the table 4. Thus, the results of the preliminary studies showed tet$(GLcN)_2Cu(Im)_2Sn_2$ complex has a stronger DNA binding propensity in contrast to tet$(GLcN)_2Zn(Im)_2Sn_2$ complex, which is well supported by the literature [43, 158].

Gel Electrophoresis

DNA Cleavage without added Reductant

To assess the DNA cleavage ability of the tet$(GLcN)_2Cu(Im)_2Sn_2$ complex, a fixed concentration of pBR322 DNA was incubated with 0.5 - 2.5 µM concentration of the complex tet$(GLcN)_2Cu(Im)_2Sn_2$ in 5 mM Tris-HCl/50mM NaCl buffer at physiological pH 7.2, for 1h without addition of reductant.

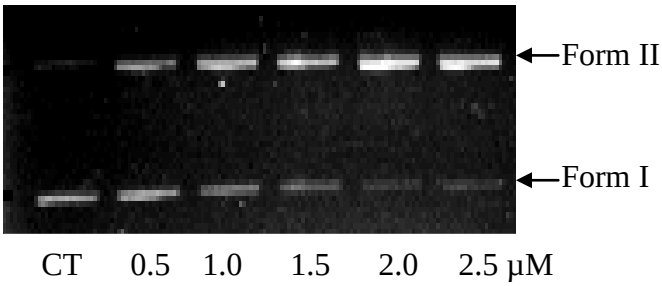

Figure 48. *The cleavage pattern of the agarose gel electrophoresis for pBR322 plasmid DNA (300ng) by tet$(GLcN)_2Cu(Im)_2Sn_2$ (0.5-2.5 µM), after 1h incubation time (concentration dependent)*

The concentration-dependent DNA cleavage activity of tet$(GLcN)_2Cu(Im)_2Sn_2$ was observed by gel electrophoresis (Figure 48) [238]. The cleavage pattern depicted conversion of supercoiled (SC form; Form I) into the nicked circular form (NC form;

Form II) with increase in concentration of tet$(GLcN)_2Cu(Im)_2Sn_2$; no conversion to linear circular form (LC form; Form III) was observed by tet$(GLcN)_2Cu(Im)_2Sn_2$, indicating that tet$(GLcN)_2Cu(Im)_2Sn_2$ is involved in single strand DNA cleavage. The results suggest that an efficient cleavage activity was exhibited by the complex tet$(GLcN)_2Cu(Im)_2Sn_2$, which corroborates well with the findings of binding studies performed spectroscopically.

DNA Cleavage with added Reductant

To examine whether reducing agents present in the reaction mixture could account for the increased DNA degradation by tet$(GLcN)_2Cu(Im)_2Sn_2$, cleavage reaction was performed in air by the addition of the reducing agent ascorbic acid to the reaction mixture containing supercoiled pBR322 DNA in 5mM Tris-HCl/50mM NaCl buffer at pH 7.2 (Figure 49). In the control experiment performed in the presence of ascorbic acid without addition of the complex tet$(GLcN)_2Cu(Im)_2Sn_2$, no cleavage was observed.

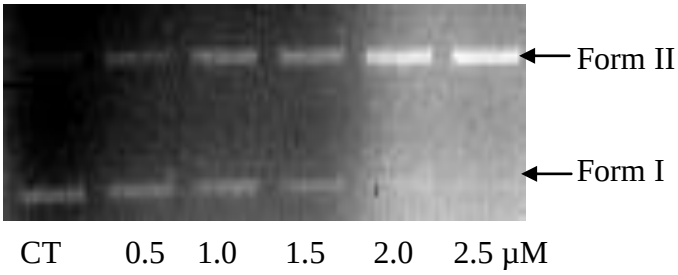

***Figure 49**. The cleavage patterns of the agarose gel electrophoresis for pBR322 plasmid DNA (300ng) by tet$(GLcN)_2Cu(Im)_2Sn_2$ (0.5-2.5 µM) in the presence of ascorbic acid, after 1h incubation time.*

With increasing concentration of complex tet$(GLcN)_2Cu(Im)_2Sn_2$ from 0.5-2.5 µM, a slight increase in the nicked circular form (NC form; Form II) of the DNA was observed in comparison to gel pattern observed in the absence of reductant. This

increase in DNA cleavage activity of complex tet$(GLcN)_2Cu(Im)_2Sn_2$ was apparently caused by enhanced stabilization of the Cu(I) species formed upon its reduction by ascorbic acid.

Photoinduced DNA cleavage

The DNA cleavage activity of the tet$(GLcN)_2Cu(Im)_2Sn_2$ complex at 0.5 - 2.5 µM concentration was studied using pBR322 DNA (~ 80% Supercoiled form) in 5mM Tris-HCl/50 mM NaCl buffer at pH 7.2 and upon irradiation with UV light of 365 nm [239]. Interestingly, tet$(GLcN)_2Cu(Im)_2Sn_2$ involves double stranded DNA cleavage to generate the linear circular (LC form; Form III), before converting (SC form; Form I) into (NC form; Form II) through single strand breaking. On increasing the concentration, tet$(GLcN)_2Cu(Im)_2Sn_2$ produces complete conversion of (SC DNA; Form I) into (NC form; Form II) and (LC form; Form III) (Figure 50).

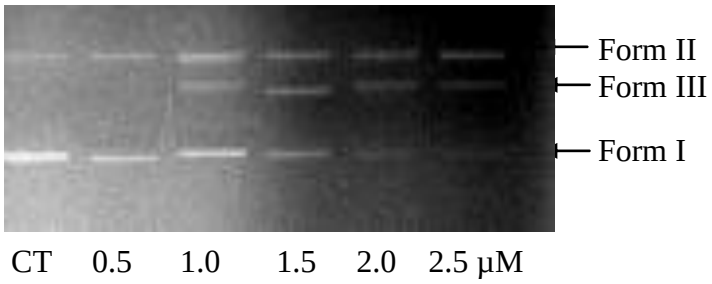

***Figure 50**. Photoinduced electrophoretic separations showing the cleavage of pBR322 plasmid DNA (300ng) induced by tet$(GLcN)_2Cu(Im)_2Sn_2$ (0.5-2.5 µM) after 0.5h incubation time, in buffer (5mM Tris –HCl/ 50 mM NaCl, pH= 7.2 at 25°C).*

Antitumor activity assays

In vitro anticancer activity of complex tet$(GLcN)_2Cu(Im)_2Sn_2$ was screened against 14 different human carcinoma cell lines of different histological origin. The Sulforhodamine-B (SRB) assay was used to assess the cellular proliferation [208].

The complex tet$(GLcN)_2Cu(Im)_2Sn_2$ exhibited cytotoxicity against Colo205 (human colon carcinoma cell line) and A2780 (human ovary carcinoma cell line). However, significantly good results were obtained against DWD (human oral carcinoma cell line) and MCF-7 (human breast carcinoma cell line).The results in terms of GI_{50} values are given in the table 5.

***Table 5**. Summary of the screening data of tet(GLcN)$_2$Cu(Im)$_2$Sn$_2$, for the in vitro anti tumor activity (**GI$_{50}$** in μg/ml).*

Cell lines	Hop62	A549	PC3	DU145	A498	DWD	Colo205	HT29	T24	MIAPAC2	MCF7	ZR-75-1	SiHa	A2780
tet(GLcN)$_2$Cu(Im)$_2$Sn$_2$	77	37	>80	33	>80	17	<10[a]	>80	60	28	22	36	40	<10$_a$
[±] **ADR**	<10	<10	<10	<10	<10	<10	<10	<10	<10	<10	<10	<10	<10	<10

Note:

***GI$_{50}$** = Growth inhibition of 50 % (GI$_{50}$) calculated from [(Ti-Tz)/(C-Tz)] x 100 = 50, drug concentration result in a 50% reduction in the net protein increase.*

[±] ***ADR**= Adriamycin (Positive Control Compound).*

[a] ***GI$_{50}$** value <10 μg/ml is considered to demonstrate activity.*

Conclusion

In the present work, we have described the synthesis and characterization of carbohydrate-conjugate heterobimetallic tet$(GLcN)_2Ni(Im)_2Sn_2$, tet$(GLcN)_2Cu(Im)_2Sn_2$ tet$(GLcN)_2Zn(Im)_2Sn_2$ complexes. *In vitro* DNA binding studies of the complexes employing UV-vis titrations, fluorescence, cyclic voltammetry and gel electrophoresis were carried out to ascertain the mode of binding and the extent of binding. The 'hyperchromic effect of the absorption intensity of the intraligand transitions reveals that both tet$(GLcN)_2Cu(Im)_2Sn_2$ and tet$(GLcN)_2Zn(Im)_2Sn_2$ complexes bind primarily by electrostatic interaction. The tet$(GLcN)_2Cu(Im)_2Sn_2$ complex exhibited an effective DNA cleavage activity under physiologically relevant conditions due to its dual binding affinity which enhances local concentration of metal complexes around DNA and consequently the better cleavage activity. tet$(GLcN)_2Cu(Im)_2Sn_2$ complex exhibits the highest anticancer activity against the Colo205 (human colon carcinoma cell line) and A2780 (human ovary carcinoma cell line). Rapid changes in nuclear morphology were noticed with Hoechst staining, which was confirmed by acridine orange/ethidium bromide staining, revealing the fact that most of the cells enter early apoptosis with increase in concentration (1-8 μM) of the tet$(GLcN)_2Cu(Im)_2Sn_2$ complex on A2780 cell lines.